UNSTEADY AERODYNAMICS OF FLAPPING FLIGHT

A THESIS SUBMITTED FOR THE DEGREE OF

Master Of Science (Engg.)

BY

BINAYA KUMAR DHAR

TO

JAWAHARLAL NEHRU CENTRE FOR ADVANCED SCIENTIFIC RESEARCH
BANGALORE- 560 064, INDIA
MAY-2003

Dedicated to
my family

DECLARATION

I declare that the matter presented in this thesis entitled **"UNSTEADY AERODYNAMICS OF FLAPPING FLIGHT"** is the result of studies carried out by me at the Engineering Mechanics Unit of the Jawaharlal Nehru Centre for Advanced Scientific Research, Bangalore, India, under the supervision of Dr. K . R. Sreenivas and that this work has not been submitted elsewhere for any other degree.In keeping with the general practice of reporting scientific observations, due acknowledgement has been made wherever the work described has been based on the findings of other investigators.

Binaya Kumar Dhar

Place: Bangalore

Binaya Kumar Dhar.

Date: 06/05/03

CERTIFICATE

This is to certify that the work described in the thesis entitled "**UNSTEADY AERODYNAMICS OF FLAPPING FLIGHT**" is the result of investigations carried out by Mr. Binaya Kumar Dhar in the Engineering Mechanics Unit of the Jawaharlal Nehru Centre for Advanced Scientific Research, Jakkur, Bangalore 560 064, under my supervision, and that the results presented in this thesis have not been previously formed the basis for the award of any other diploma, degree or fellowship.

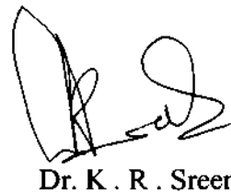

Dr. K . R . Sreenivas

Acknowledgements

I take this opportunity to express my gratitude to my research supervisor, Dr. K.R.Sreenivas for his invaluable guidance and moral support, which have been instrumental in making my transition from an engineer to a research scholar smooth and successful. The constant encouragement that I received from him has helped me to appreciate the art of science, analysis and tackling of a scientific problem. The enormous intellectual freedom that I enjoyed in his laboratory during the course of these studies will be cherished. I would like to thank our chairman Prof. Roddam Narasimha and Dr. Rama Govindarajan for their advice and encouragement throughout my stay.

I would like to thank people at CES (IISc) and GKVK for guidance in catching and preservation of insects while performing experiments using insects.

I am being greatly owed to my co-researchers Pradeep Bhat , Shrikrishna M. Badiger, Faraz Mehdi and Mukund for their excellent contribution starting from preparation of butterfly model upto the end of flow visualization. Without help from these people never I would have dreamt of reaching upto this limit. I would like to thank Murli and Aanish of Fluid Mechanics Lab of IISc for their valuable suggestions while doing flow visualization experiments.

I wish to express my gratitude to all academic as well as the non-academic staff of JNCASR for their help throughout my stay. I am greatly thankful to Mr. Arogyanathan of our M/C shop for helping me in fabrication work.

I have enjoyed the company of lab mates Siva, Saji, Nvinod, Sameen, Dr. Sanjeev Rao, Saurav, Mukund, Faraz, Srikrishna, Antina, Subarna and kirti. Special thanks to Nvinod, Sameen, Saurav, Vijay, Priyaranjan, Shreyas and Shreenath, Rajesh Khanna, Kavitha siva, Ram shankar, Jammal, Arpita, Lakshmi, Siddapa, Prasant dash, Complab, Shailesh and Gargi raina for taking enormous troubles while doing work as well as while writing my thesis. I am grateful to all of them for their patience with my whims and fancies. I am also thankful to all students of JNCASR for their constant support during my stay.

I enjoyed the friendship of a large number of people in the Indian Institute of Science (Rasmi, Niladri, Santosh, Sangram, Sisir, Niranjan, Subhasish, Paresh and Om prakash) as well as all of my batch mates here in Bangalore. I am grateful to all of them.

List of figures

Fig. No.		Page No.
1.1	As the size of the insect/bird decreases the flapping frequency increases this seems to suggest that the nature favours unsteady aerodynamics for lift-generation at small sizes (low Reynolds-numbers) as shown in Figure	2
1.2	Figure shows, Γ grows towards the predicted Γq instead of the maximum value Γmax limited by steady stall, until the first signs of stalling are detected. (Ellington, 1984)	3
1.3	Figure shows the Flow visualization of the leading edge vortex over the wing of a flapper during the middle of down-stroke. Smoke was released from the leading edge. The camera view is parallel to the wing surface.(Ellington 1999)	4
1.4	Figure shows the flow field around a model wing during "fling". Note instantaneous formation of vortices as the wing is opening. As the flow rushes into the gap between the opening-wings, an instantaneous lift is generated (Maxworthy 1979)	5
1.5	Figure shows the Interaction of the model-wing with the wake of previous stroke; phasing of the wing rotation with the end of previous stroke and actual orientation of the wing can be used to produce enhanced lift and to achieve high maneuverability (Dickinson, et. al. 1999)	6
2.1	Figure shows the Schematic diagram of the bevel-gear assembly	8
2.2	Schematic diagram indicating complete setup with an inset photo of the bevel-gear assembly	9
2.3	Photo of the flapping test-rig with transparent wings and a stepper motor	9
2.4	Schematic diagram indicating wing motion, displacement and angular velocity for different strokes (Clap and fling, Symmetric and Asymmetric)	10
2.5	Sets of wings used in the experiments (shown at 1:5 scale). Red lines indicate dye injection locations	11
2.6	Figure shows the flow fields observed during clap and fling motion of the model wings. (a)Indicates the flow filed just after opening of the wings (beginning of the fling motion) and (b) at the end of the fling stroke. Blue lines indicate the fluid motion and the green–lines indicate direction of the force generated during fling (Re=1070)	11
2.7	Figure shows the Gradual development of flow structure during the clap and fling motion of the wing (a) in the middle of the fling-stroke, (b) just after the end of fling-stroke (c) during clap-stroke and (d) resultant flow structure after many clap and fling strokes. Blue arrows indicate typical flow directions.	

	Green arrows are forces generated during fling-stroke (solid arrow) and clap-stroke (broken-arrow). Photos are for small-wing	12
2.8	Flow features for clap-fling motion for a bigwing. (similar to Figure 2.7). Reynolds number is 1070. Blue arrows indicate directions of fluid flow after many cycles of clap and fling motion	12
2.9	Figure shows the flow field around the big wing at Re = 2420. Top panel indicates the flow filed after many cycles of wing motion, vortex ejected at the end of clap is evident	13
2.10	Figure shows the flow fields around flapping wings, with symmetrical velocity profiles; a, b and c for big-wing and d, e and f for small-wing. Vortices shed at the end of each strokes are evident in a and c for big wing and in d, e and f for small wing. In f, a vortex shed in previous stroke (shown in inset) has moved to circled area (right bottom corner) while a new vortex is just shed at the other end. Blue arrows indicate the direction of the fluid flow and black arrows in the top panel indicate the motion of the wing	13
2.11	Flow visualization pictures for the case of flapping wings with asymmetric velocity profiles. a during down-stroke and b at the end of down-stroke (Re=1070) and c (Re=750) at the end of upstroke. d is at the end of upstroke (for this experiment down-stroke Re=1520 and upstroke Re =465). Pink square area indicates well developed vortex during down-stroke and pink circle indicates the absence of a well defined vortex. Blue arrows indicate direction of fluid flow, black arrows indicate direction of wing motion	14
2.12	In this figure flow field for a flapping wing with asymmetric velocity profiles (Re-1070-750), after many cycles of operations. Unlike in symmetric flapping, in this case asymmetry in the flow field is clearly evident. Almost all the fluid is displaced in the direction of the blue-arrow starting from upper left corner to the lower right corner. As a result, flow from both wings would produce a net lift force in the direction of the red arrow	15
3.1	Figure shows the schematic diagram indicating arrangement to get top and back views of insect flying in wind tunnel	18
3.2	Figure shows the simultaneous recording of top and back views of an insect in the wind tunnel	19
3.3	Figure shows schematics of constant-temperature hot-wire anemometer.	21
3.4	This shows the Schematic diagram indicating pendulum arrangement for calibrating hot-wire in the low velocity range	22
3.5	Figure shows that setting of the probe distance depending on the desired velocity	23

3.6 Figure shows the variation of probe output (voltage) with the velocity of the probe 24

Synopsis

In the thesis we present a study on the unsteady aerodynamics of insect flight. Motivation for the study is to establish the rational for adopting unsteady aerodynamics principles in the design of Micro Air Vehicles (MAV) and to develop engineering design guidance for the same. Unlike an aircraft with fixed wing or a propeller, birds and insects reciprocate their wings changing the wing direction and the pitch twice in each stroke. Birds and insects generate lift based on unsteady aerodynamic principles. Birds in flight, unlike many insects, not only change their wing direction and pitch but also change the wing area and wing porosity during a stroke. Thus an insect flight is an order less complex for adaptation to a MAV application compared to the bird flight and hence we restrict our discussion here only to insect flight.

Study of insect flight is challenging as it involves measurement of small forces cycling at high frequency. Typical forces in the case of a tiny insect like fruit fly will be a fraction of mg cycling at 200Hz or more and at the other end of spectrum, for big insects, like butterfly and dragonfly forces will be in the range of 1-2 gm cycling at 5-40Hz. Study of wing kinematics is also challenging as we need to get at least two simultaneous-views of a flying-insect at high frame rate (frame rate has to be at least 10 to 15 times more than the wing beat frequency). From these two views, we have to workout actual orientations of the wing and its variation in time. Keeping these factors in mind, we have developed a two-pronged approach for the study of insect flight dynamics. In one approach, we make a mechanical model, to mimic some salient features of insect flight and carryout flow visualization. In the second approach we are developing tools to study the wing kinematics of an insect while in flight.

The thesis has following outline. In the first chapter, we describe some salient features of unsteady aerodynamics principles, low Reynolds number flight, how insect uses unsteady aerodynamics principles for its flight, desirability of adopting insect flight for MAV design. In this chapter we also give scope of the present work.

In the second chapter we present the design of one-degree freedom model, mimicking insect flight, control system used to drive this model, design of flow visualization setup, test section, flow visualization pictures and discussion based on the flow visualization results.

In the third chapter we present some of the preliminary arrangements developed to get wing-kinematics of an insect while in flight. This includes camera system for getting simultaneous front and top view of a flying insect in a wind-tunnel. As the actual flight speed of insect is about 1m/s, we have to keep low wind speeds in the wind tunnel and in this chapter we present a procedure for calibrating anemometer in low wind speed regime.

In the fourth chapter we present conclusions and scope for future work.

Contents

Declaration		**i**
Certificate		**ii**
Acknowledgement		**iii**
List of figures		**iv-vi**
Synopsis		**vii-viii**
Chapter1: Introduction to the problem		
1.1	Bird and Insect Flight	1-2
1.2	Why we need to study Insect Flight?	2
1.3	Unsteady Mechanisms of Insect Flight	2-3
1.3a	Delayed Stall and Wing Rotation	3-4
1.3b	Clap and Fling Mechanism	4-5
1.3c	Wake Capture	6
1.4	Scope of Present Work	6-7
Chapter 2 : Flow Visualization of butterfly model		
2.1	Mechanical Model to Mimic Insect Flight(Test-rig)	8-9
2.2	Experiments	10-11
2.3	Flow Visualization	11-16
Chapter 3 : Experiments with insects		
3.1	Introduction	17
3.2	Camera arrangement for studying wing-kinematics	17-19
3.3	Preservation of insects	20
3.4	Hot wire anemometer calibration	20-24
Chapter 4 : Conclusions and scope for future work		25
Appendix		26-29
References		30-31

Chapter 1: Introduction

1. 1 Bird and Insect Flight

In nature, birds and insects have mastered the airspace and their flight has fascinated humans for many centuries. Many birds routinely experience positive G-forces in excess of 10Gs and up to 14Gs whereas most general aircrafts experience a maximum permitted positive G-force of about 5Gs and military aircraft withstand 8-10Gs. With respect to maneuvering a body through space, insects represent one of the nature's finest locomotion experiments, e.g. dragonfly, humming-birds and even a house fly (which make them difficult to swat!).

Insects alone are capable of wide varieties of flights. We have low wing-beat frequency gliding flight (butterfly) to a flight with very high wing-beat frequency (Diptera: Ceratoponidae, about 1000 Hz, [Sotavalta, 1947]). It has been reported that a male insect (Diptera: Tabanidae) can reach a speed of about 140 km/h in pursuit of a female insect[Wilkerson, and Butler, 1984]. In terms of the insect's body length, Diptera's speed will be more than 1000 body lengths per second and compare this with the speed of a supersonic aircraft traveling near Mach 3, which is just about 32 body lengths per second. Many insects, for example dragonflies, are capable of taking off backwards, hovering, flying forwards at a speed of 100 body lengths per second, flying backwards (speed more than 3 body lengths per second), flying sideways and landing upside down. Insect flight also covers a wide range of Reynolds number from approximately 10 for the smallest insects to about 10^4 for large insects like beetles, moths and butterflies.

Unlike an aircraft with a fixed wing or a propeller, birds and insects reciprocate their wings changing the wing direction and the pitch twice in each stroke. They generate their lift and thrust by unsteady aerodynamics. As they operate at relatively low Reynolds numbers, wing profiling is not required and unsteady aerodynamics seems to be more efficient for lift generation. Bird and insect flight also present an ingenious control system in complex unsteady flows. The interaction between the wings and the surrounding flows produces a robust flying mechanism, which is far more advanced in certain respects than current technology. An important difference between hovering and forward flight is that while hovering insects fly in unsteady and complex vortical flows, generated by flapping and rotation of their wings. The starting and stopping vortices from both the leading and trailing edges interact non-trivially to produce a high lift.

Some of the lift generating mechanisms using unsteady aerodynamics are (a) delayed stall [Ellington,1984 and Maresca et. all, 1979](b) wake capturing [Dickinson et. all, 1999] (c) wing rotation [Ellington,1984 and Dickinson et. al.,1999] and (d) clap and fling mechanism[Weis-Fogh,1973 and Maxworthy,1979]. An insect uses a combination of the above mechanisms for its flight and achieves high maneuverability by manipulating surrounding unsteady fluid motion. Birds in flight, unlike many insects, not only change their wing direction and pitch but also change wing area, shape and porosity during a stroke. Insect flight being much less complex than bird flight is the right point for research into flapping flight aerodynamics.

Two points are clear from the above discussion: firstly, at the scales on which birds and insects operate, and from the points of view of efficiency, control and maneuverability, flapping flight offers many advantages over more conventional aircraft with fixed wings, propellers and/or rotating helicopter-like blades. Secondly, flapping flight is more complicated than flight with fixed wings. Coupled with this technological limitations forced

the inventors in the 20th century to abandon flapping- flight configuration. With many years of research, principles of steady aerodynamics (2-D aerofoils and finite wings) applicable to a fixed wing aircraft are quite well understood. *In contrast, the engineering principles needed for an optimum design of small mechanical objects which can use unsteady aerodynamics for propulsion and lift have not yet been established.* Therefore, there is a need for systematic and comprehensive study of the principles of unsteady aerodynamics which pertain to the fluid dynamical problem of flapping flight, in order to both understand the rationale for its use in nature and to obtain design-guidelines to exploit unsteady aerodynamics for flight.

1.2 Why We Need to Study Insect Flight?

As the size of the insect/bird decreases the flapping frequency increases this seems to suggest that the nature favours unsteady aerodynamics for lift-generation at small sizes (low Reynolds-numbers) as shown in Figure 1. As discussed in the earlier section, for a small size aircraft, there are many advantages in adapting unsteady aerodynamics of insect flight for lift and thrust generation. The specified dimensions for a MAV are: maximum size of 15 cm in any direction, 100 g takeoff load and flight speed of 5-20 m/s with a flight endurance of about 30 minutes. Unlike a micro-air-vehicle based on the fixed wing design, insect based design gives the capability of hovering, high maneuverability and based on the observed trend in nature, it may be efficient mode of flight for a small scale aircraft. These capabilities will make a micro-air-vehicle with unsteady aerodynamics an attractive

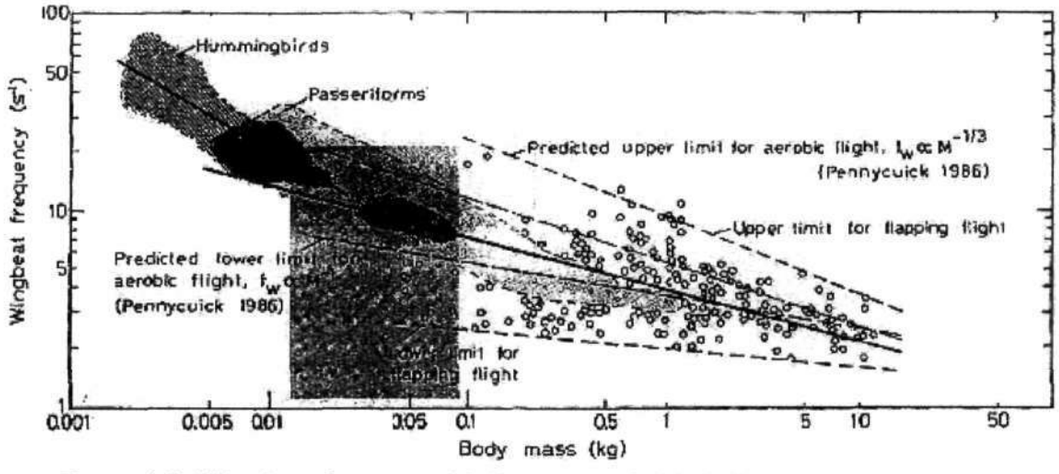

Figure 1.1: Wing beat frequency Vs Body mass in birds. The shaded region indicates the expanded parametric range surrounding the projected size, speed and weight for MAV (**Shvy et. al., 1999**)

proposition for following applications:

1. Aerial photography.
2. 'Sniffing' in hazardous environment.
3. Policing in cities: Monitoring traffic and mobs.
4. Search and rescue operation.

1.3 Unsteady Mechanisms of Insect Flight:

In this section we will highlight many of the unsteady aerodynamics principles that an insect exploits while in flight. For achieving flapping flight four degrees of freedom are used in nature. They are flapping, feathering, lagging and spanning.

Flapping: It is an angular movement about an axis in the direction of flight.

Feathering: It is an angular movement about an axis at the center of the wing that tilts the wing changing its angle of attack.

Lagging: It is an angular movement about a vertical axis that effectively moves the wing forward and backward parallel to the body.

Spanning: It is the expansion and contraction of the wing span.

An insect many not use all the degrees of freedom for its flight, many insects use a combination of the motions subjected to their physiological restriction to get maximum benefit. Insects do not use spanning; also they have a very restricted lagging capability. In effect the wing motion of an insect is composed of flapping and feathering.

Wing kinematics of an insect can be divided typically into four parts. Two translational motions (upstroke and down-stroke) with a rotational motion at the end of each stroke. During the translation the wings sweep through the air with large angles of attack and during rotation the wings rotate and change their direction. The rotational motion is what referred to as feathering in the above paragraph. Wing kinematics is the function of the following variables: ***wing beat frequency***, ***wing-beat amplitude*** and ***wing feathering*** as a function of wing position.

a. Delayed stall and wing rotation
b. Clap and Fling
c. Wake Capturing

1.3a Delayed Stall and Wing Rotation:

Stalling is a phenomenon in which an aerofoil moving with large angles of attack will lose the lift due to flow-separation over the wing surface. When a wing starts moving in air, circulation and lift will start developing, if the angle of attack (α) is large, the flow over the wing surface will separate and stall occurs. Let us say the steady state angle-of-attack at which separation occurs be α_s. An airfoil can travel several chord lengths at large angles of attack ($\alpha > \alpha_s$) before the separation associated with stall begins, & large transient circulation can be developed during that period (Wagner effect). The enhanced circulation must eventually be lost as the flow separates from the upper surface & steady case is realized. If the insect completes its stroke before the onset of stall, it can enjoy higher lift than the steady state value. Thus insects exploit the unsteady aerodynamics principle of delay in onset of stall. To put it in a simpler way, the insects maintain lift even when they beat their wings with high angles of attack and generate lift more than the steady state value.

Γ = Circulation and λ = Non- dimensional distance.

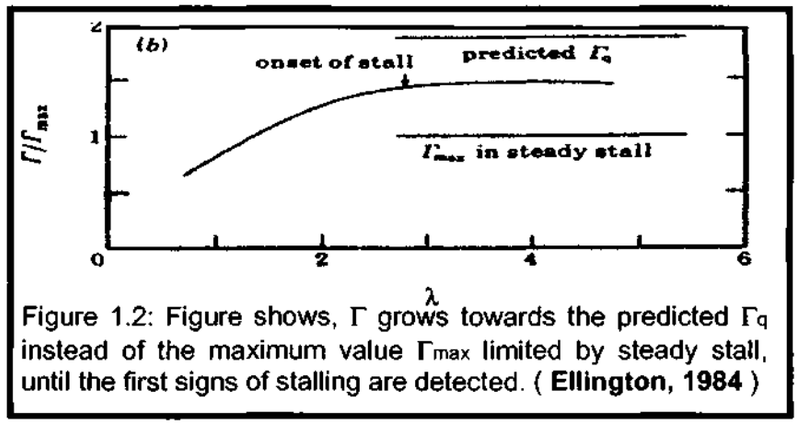

Figure 1.2: Figure shows, Γ grows towards the predicted Γ_q instead of the maximum value Γ_{max} limited by steady stall, until the first signs of stalling are detected. (**Ellington, 1984**)

Wing rotation, the dynamic change in the angle of attack will also delay the onset of stall. If the wing, as it moves forward is pitching continuously (dynamically changing angle of attack), it can for a short-interval exceed the angle of attack α_s without having flow-separation and generate a lift higher than the steady state value. Additional circulation due

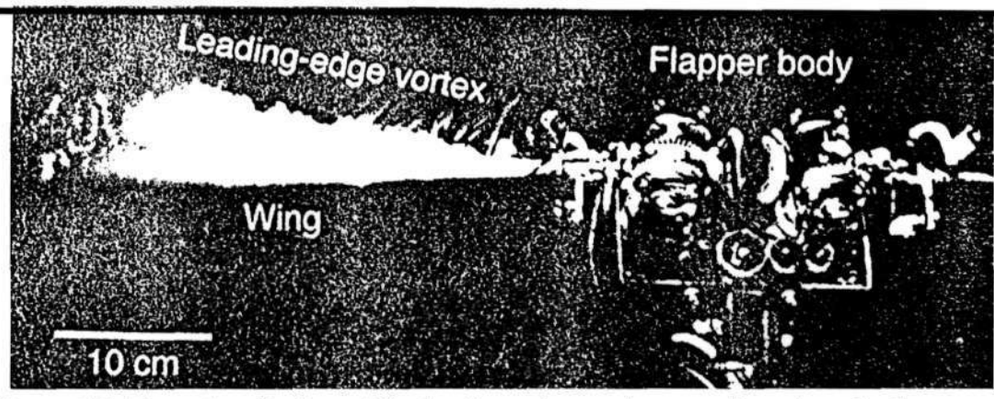

Figure 1.3: Flow visualization of the leading edge vortex over the wing of a flapper during the middle of down-stroke. Smoke was released from the leading edge. The camera view is parallel to the wing surface (**Ellington, 1999**)

the wing-rotation (by continuously changing angle of attack during a stroke) will stabilize the flow on the upper surface of the wing that will delay the flow-separation and onset of stall (Kramer's effect). Apart from the lift due to wing-translation, rotation of the wing will also add circulation and hence additional lift (Magnus effect). Rotational lift will be the only component of lift at the end of each stroke when wing comes to rest and changes its direction of motion.

In some cases, a leading edge vortex will pump the air along the axis of the wing; the upper surface flow gets stabilized and will delay the onset of stall [leading edge vortex stabilization, (Ellington, 1999)].

1.3b Clap and Fling Mechanism:

The first unsteady mechanism for lift generation was identified by Weis-Fogh (1972, 1973) and is known as **`clap and fling'** mechanism or **Weis-Fogh** mechanism. Weis-Fogh used clap and fling mechanism to explain the high lift generation in the chalcid wasp, *Encarsia formosa.* A detailed theoretical analysis of the clap-and-fling can be found in Lighthill (1973), and experimental treatments in (Maxworthy, 1979) and (Spedding & Maxworthy, 1986). Small insects and butterfly use clap and fling mechanism for their lift generation. Figure given bellow, indicates the flow filed around a model mimicking fling motion (Maxmorthy, 1979). One of the main advantages of this mechanism is that the lift generation is instantaneous; when a butterfly opens its wings (fling them apart) it will be immediately airborne. The kinematics is simple compared to many other insects, for example dragonfly;

however, the lift generated is highly unsteady which results in an erratic flight path as observed in many butterflies.

Figure1.4: Flow field around a model wing during "fling". Note instantaneous formation of vortices as the wing is opening. As the flow rushes into the gap between the opening-wings, an instantaneous lift is generated (**Maxworthy, 1979**).

1.3c Wake Capture:

Rotational circulation can not explain the large positive transient that develops immediately after the wing changes direction at the start of each half stroke (Dickinson et. al., 1999). In wake capture, the Wing benefits from the shed vorticity of the previous stroke. The flow generated by one stroke can increase the effective fluid velocity at the start of the next stroke & thereby increase the force production above that which could be explained by translation alone. Wake capturing is a mechanism by which insect extract energy from the wake shed by previous stroke augments its lift in the beginning of a new stroke thus improving the overall efficiency. Wake capture mechanism is also exploited to achieve a high maneuverability by manipulating with wing rotation and translation.

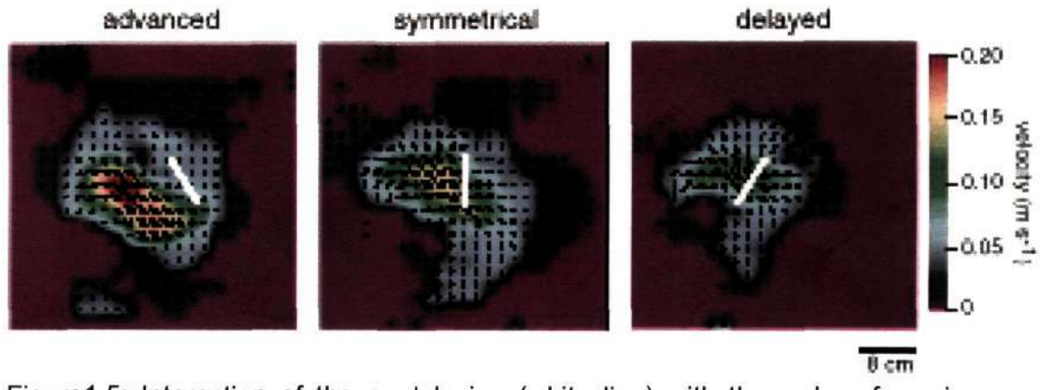

Figure1.5: Interaction of the model-wing (white line) with the wake of previous stroke; phasing of the wing rotation with the end of previous stroke and actual orientation of the wing can be used to produce enhanced lift and to achieve high maneuverability (**Dickinson, et. al., 1999**).

1.4 Scope of the Present Work.

Current interest in the insect flight is motivated by two factors: (1) as a plausible mechanism for adapting into micro-air-vehicle (MAV) development and (2) fundamental curiosity to understand low Reynolds number unsteady aerodynamics. The Defense Advanced Research Agency (DARPA) of USA has set a design target to develop a MAV which has maximum dimension of 15 cm in any direction, with cruise velocity of 0-20 m/S, flight endurance of 30 minutes, all-up weight of 100 gms and having a range of 2-10kms. This definition clearly puts MAV into low Re flight-application (Re $\approx$ 20 000). In nature, as the size of the insect (or bird) decreases they beat their wings higher frequencies to generate their lift, conversely large birds like vulture glides like an aircraft with fixed wing. Thus trend in nature is to move towards unsteady aerodynamics for lift generation as the size (or weight) decreases. Unanswered question is that, is it more efficient to adapt flapping flight at smaller-scales (as in the case of MAV), a trend that observed in nature?

Previous studies on the insect-flight can be broadly divided into following areas: (a) wing kinematics and force measurement of an insect while in flight (Dragonfly-Wakeling and Ellington, 1997; Fruit flies - Zanker, 1990, Lehmann and Dickinson, 1998; moth-Wilkin and Williams, 1993 and desert locust-Wortmann and Zarnack, 1993) (b) theoretical analysis, modeling and numerical simulations (Lighthill, 1973; Weis-Fogh, 1972 and 1973; Ellington, 1984 a, b and c; Shyy et. all., 1999; Liu and Kawachi, 1998; Jane Wang, 2000) and (c) study on mechanical models (Maxworthy, 1979; Spedding and Maxworthy, 1986; Dickinson et. al., 1999). Designing an efficient MAV will be an interdisciplinary effort. Because of the size and weight restrictions, many components used will have multiple-functions: for example, MAV-wing apart from lift generation may also require to functioning as a solar panel for energy, as an antenna for telemetry. Other enabling technologies required would be a suitable power plant, MEMs based accelerometers and controllers, and lightweight chip based cameras. We however, restrict our discussion only to the aerodynamic aspects of the insect flight in this thesis.

Even though the literature on this topic dates back to early 1970s covering many areas as mentioned above, we find that there are many unanswered question before adapting unsteady aerodynamics into low Reynolds number flight. Design engineering needs to know for a given application, knowing payload and size restriction of an MAV what are the best wing-kinematics, wing shape and wing-beat frequency to have an efficient MAV system. Hence the research in this area should have multi-pronged approach:

(a) Study of the wing-kinematics of different insects while in flight with forces measurement;
(b) Study of the instantaneous velocity fields produced by a flying insect; and
(c) Mimicking various wing-kinematics of insects using a mechanical model (test-rig) with an aim to identify an optimal wing motion with minimum degrees of freedom that could produce lift and thrust.

In this thesis we present a test-rig which can be used for flow visualization and for testing wing-kinematics with one degree of freedom. We have also developed an arrangement, which can be used to study wing-kinematics of insects while in flight in a wind tunnel. In the next chapter we describe the test-rig and present some of the flow visualization pictures obtained using this test-rig. In the third chapter we present the some the preliminary work done for study of insect flight in the wind tunnel. In the last chapter we present the conclusion and scope for future work.

CHAPTER 2 : Flow Visualization

2.1 Mechanical Model to Mimic Insect Flight (Test-Rig):

Mechanical model is useful in getting flow-visualization and later velocity fields while mimicking insect wing-kinematics. It is highly desirable to scale up the mechanical model and operate at lower frequencies compared to a real insect. Larger flow field associated with a bigger model will be easy to study by flow-visualization and for getting detailed velocity field. Lower frequency also helps in the study of flow-dynamics by recording the flow-field at a lower frame rate.

For the Mechanical model mimicking insect flight, we need to match following factors between flying insect and the model.

(1) Reynolds number (Re) indicates the ratio of inertial force to viscous force for the system. $Re = UR/\nu$. Where U is the average velocity of the wing tip, R is the length of the wing and ν is the kinematic-viscosity or $Re = 2\theta R^2 n/\nu$, where θ is the wing-beat amplitude and n is the wing-beat frequency.

(2) Advance ratio (A), ratio of the forward velocity to the mean-wing-tip velocity.

(3) Geometric similarity of the wing.

Present model developed by us has basically three parts: (a) driver and controller, (b) test-rig to produce flapping motion and (c) test section with recording facility. Controller consists of Indexer-LPT software on a PC interfaced to a 5 axis driver through printer ports (LPT port /parallel port of the PC) controlling five stepper motors.

One of the stepper motors is connected to a bevel-gear assembly (Figure 2.1), through a flexible coupling. The stepper motor drives bevel-gear assembly, which steps-down the speed by a factor of two and drives two coaxial shafts in opposite directions. At the other end of the coaxial-shafts, we attach model-wings. By driving the stepper-motor in clockwise and counter-clockwise direction we can impart flapping motion to the wings, see figures 2.2 and 2.3.

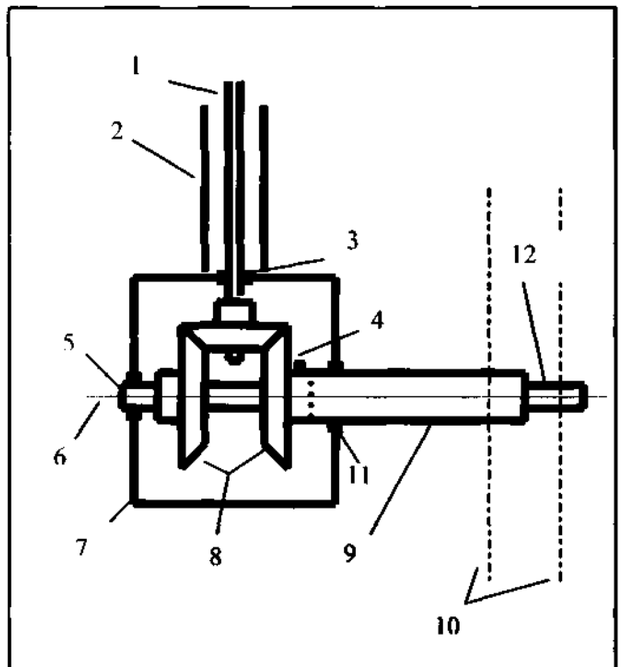

Figure 2.1: Schematic diagram of the bevel-gear assembly. 1- Drive from the motor, 2-Protecting hood and support for the drive, 3-Bush, 4-Screw, 5-Upper bound for inner solid shaft, 6- Axis of inner solid shaft, 7- Casing, 8- Bevel gears, 9- Hollow outer shaft, 10- Model wing attachment location, 11- Bush, 12-Inner Shaft

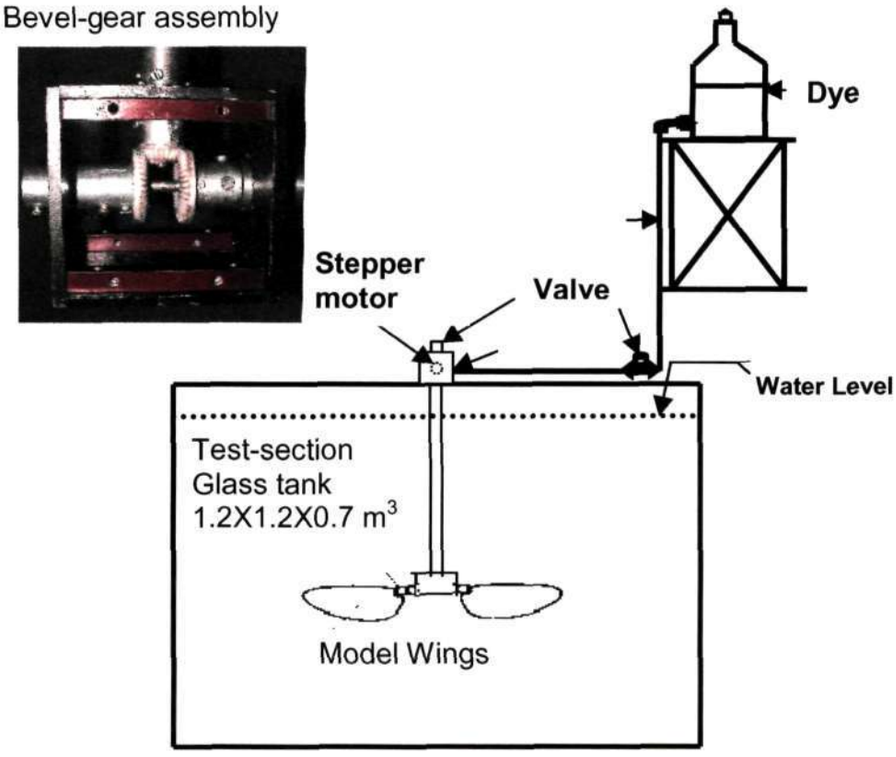

Figure 2.2: Schematic diagram indicating complete setup with an inset photo of the bevel-gear assembly.

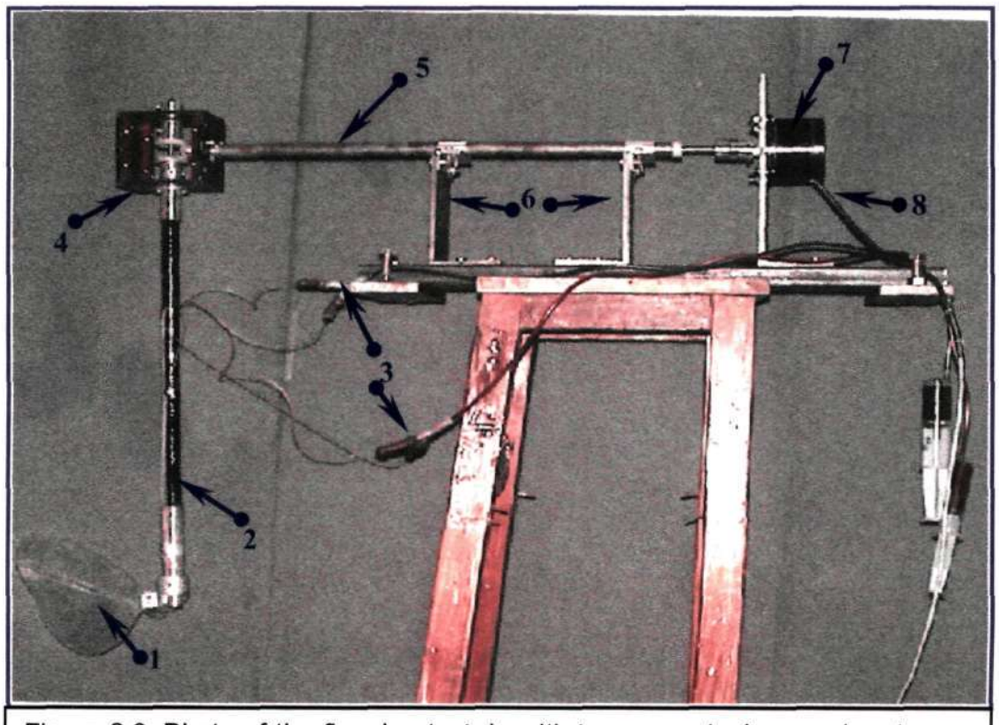

Figure 2.3: Photo of the flapping test-rig with transparent wings and a stepper motor.1-Transparent butterfly wings, 2-Shaft for transmitting the differential output to wings, 3-Dye injecting system, 4-Differential, 5-Power transmission shaft, 6-Support structure, 7-Stepper motor, 8-Control and power cables

2.2 Experiments:

We used $KmNo_4$ solution as a dye for the flow-visualization. Dye is stored in an overhead tank and a set of IV-tubes carries this dye to the wing tips (see Figures 2.2 and 2.3). Needle valves control the flow-rates and hence exit velocity of the dye at the wing tip. During experiments, flow rate of the dye is adjusted so that it follows the vortical-structures produced by the model wing. In these sets of experiments, we used a scaled-up butterfly wings as the model wings. Wings from a butterfly were scanned and enlarged to get two sets of wings having characteristic wing lengths (a) 9.9 cm (big-wing) and (b) 7.0 cm (small-wing). Characteristic wing length, R, is related to the wing area, A; $R = \sqrt{2A/\pi}$. Model

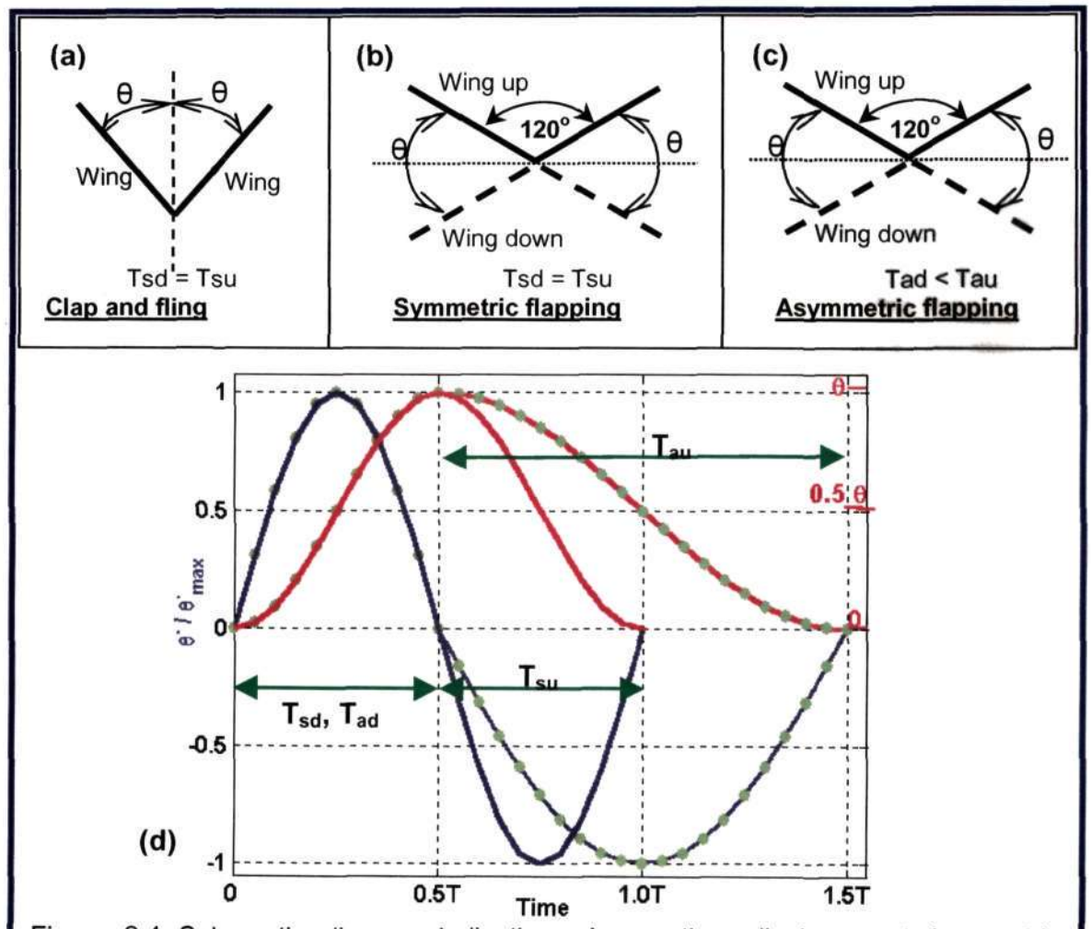

Figure 2.4 Schematic diagram indicating wing motion, displacement (symmetric stroke ——; asymmetric stroke —●—) and angular velocity (symmetric ——— asymmetric —●—) variation with time are shown. Time for symmetric down-stroke (Tsd), symmetric upstroke (Tsu), asymmetric down-stroke (Tad) and asymmetric upstroke (Tau).

wings attached to test-ring are driven in following configurations as indicated in the Figure 2.4 a, b, and c:

(a) Clap and fling motion, $\theta = 60^{\circ}$ (clap and fling stroke has same angular velocity)

(b) Symmetric flapping, $\theta = 60^{\circ}$ (same speed upward and downward stroke).

(c) Asymmetric flapping, $\theta = 60^{\circ}$ (upward and downward stroke has ***different speeds***).

In Figure 2.4 we present three configurations considered for the wing motions in the present study. Angular displacement and the angular velocity variations are shown in the Figure 2.4d. In Figure 2.5 two sets of scaled-down (1:5 scale) wing-shapes used in our experiments are shown.

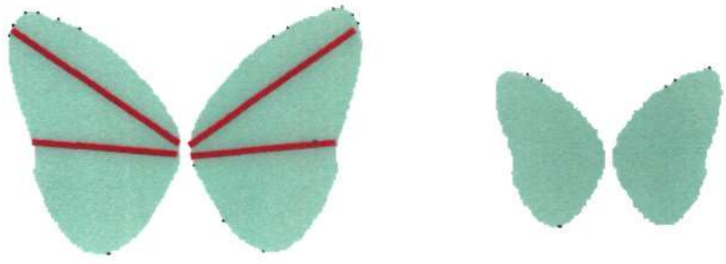

(a) Big wing; R=9.9 cm (b) Small wing; R=7 cm

Figure 2.5: Two sets of wings used in the experiments (shown at 1:5 scale). Red lines indicate dye injection locations.

2.3 Flow Visualization:

In this we present general flow fields obtained for three configurations of wing motions considered in the present study. In the first part we describe the common features observed, second part we present the comparison between these flow fields highlighting the differences observed and finally we present the conclusions drawn on the one-degree freedom system for lift generations.

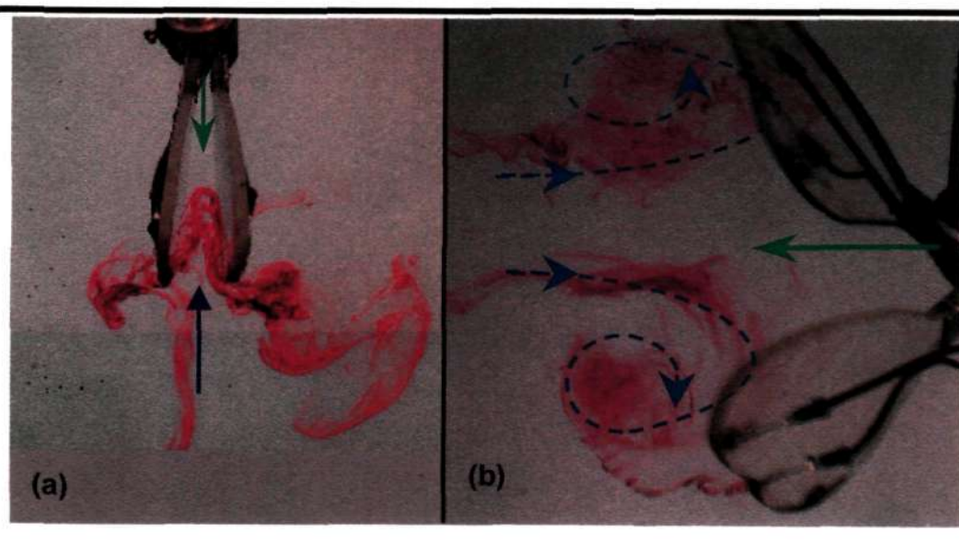

Figure 2.6: Flow fields observed during clap and fling motion of the model wings. (a) Indicates the flow filed just after opening of the wings (beginning of the fling motion) and (b) at the end of the fling stroke. Blue lines indicate the fluid motion and the green –lines indicate direction of the force generated during fling (Re=1070).

Figure 2.6 shows the typical flow fields in the clap-&-fling motion. Figure 2.6a, clearly indicates fluid rushing into the gap as the wings move apart. This type of flow is responsible for the instantaneous lift-generation as in the case of a butterfly. At the end of the fling-stroke one can see well-developed vortices in between the wing region.

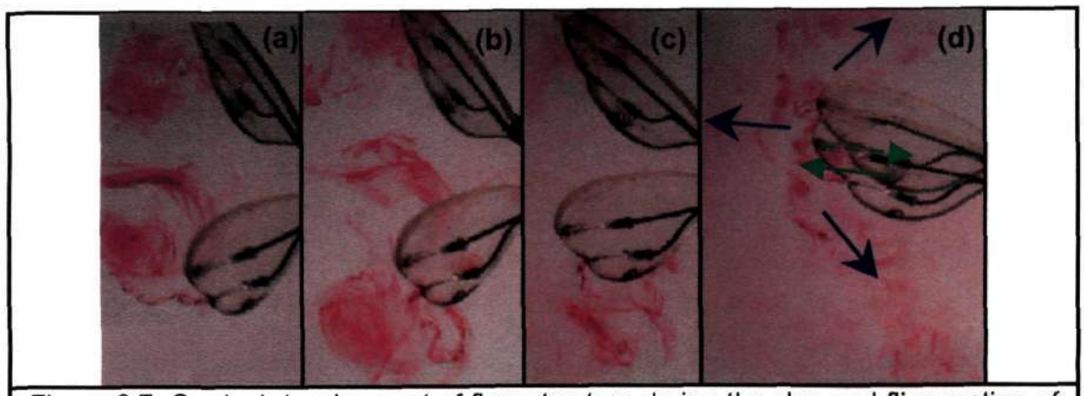

Figure 2.7: Gradual development of flow structure during the clap and fling motion of the wing (a) in the middle of the fling-stroke, (b) just after the end of fling-stroke (c) during clap-stroke and (d) resultant flow structure after many clap and fling strokes. Blue arrows indicate typical flow directions. Green arrows are forces generated during fling-stroke (solid arrow) and clap-stroke (broken-arrow). Photos are for small-wing.

Figure 2.7 shows a gradual development of the flow structure during clap and fling motion of a set of wings. Vortex structure during the fling stroke (Figure 2.7 a) develops till the end of the stroke, it will detach (Fig. 2.7 b) and is shed as the wing starts clap-stroke (Fig. 2.7c). Resultant flow structure after many cycles of operation is indicated in Figure 2.7d. Flow-streams in general are intermittent and will be primarily in three directions as indicated by blue arrows.

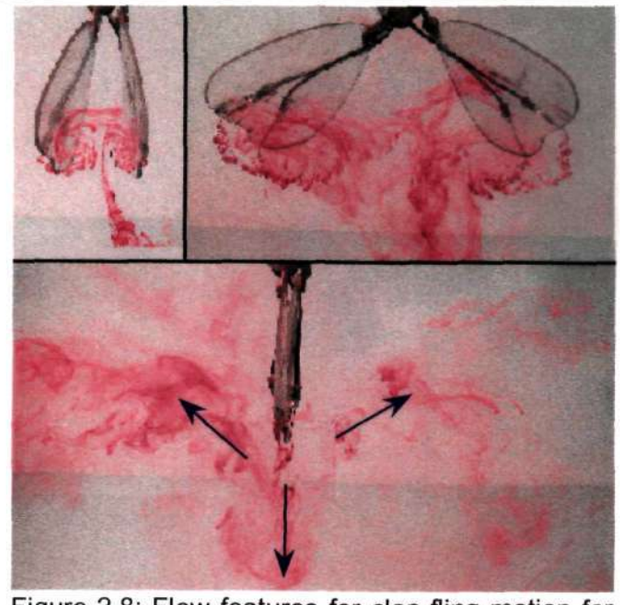

Figure 2.8: Flow features for clap-fling motion for a big-wing. (similar to Figure 2.7). Reynolds number is 1070. Blue arrows indicate directions of fluid flow after many cycles of clap and fling motion.

An accurate statement on the mean-lift force generated during a cycle will be possible only after measuring instantaneous forces or by measuring velocity fields in a complete cycle. However to a first order, by looking at the symmetry of the flow structure, we can state that the mean-lift force generated during a complete cycle is not appreciable. (The lift force that generated during

fling-stroke, solid arrow, opposes that during clap-stroke, broken-arrow). Similar flow fields are observed for big-wing operating at Re of 1050 (Figure 2.8). At higher Reynolds number of 2420, even though flow structure remains similar (Figure 2.9, bigger wing) flow looks fuzzier due to mixing and diffusion associated with higher Reynolds number. In Figure 2.9 again three streams of flow are evident with a well-formed vortex ejecting at the end of clap-stroke.

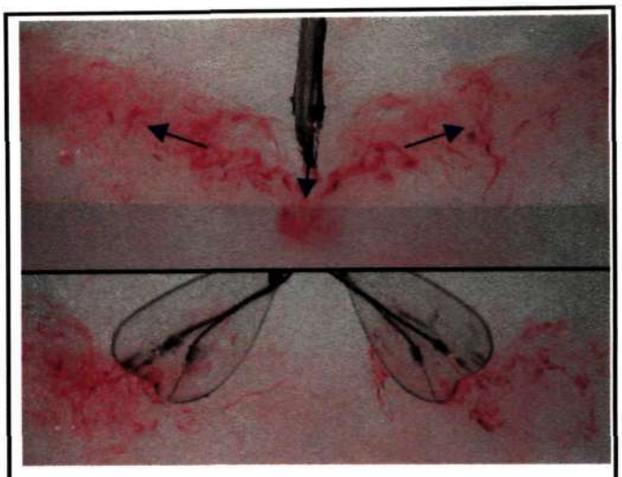

Figure 2.9: Big-wing at Reynolds number 2420. Top panel indicates the flow field after many cycles of wing motion, vortex ejected at the end of clap is evident.

Next set of experiments done was with a configuration in which each wing flaps up down; the amplitude of the motion is 60° (left wing from 150^{0} to 210° and right wing from 30^{0} to -30^{0}). Angular velocity is symmetrical, as indicated by solid blue line in Figure 2.4d.

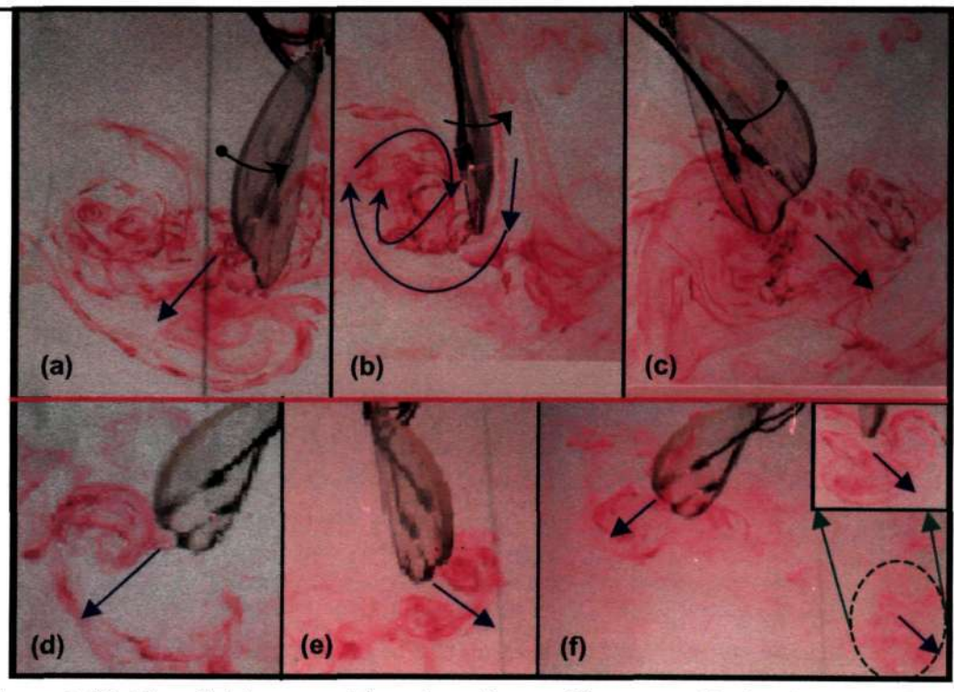

Figure 2.10: Flow fields around flapping wings, with symmetrical velocity profiles; ***a***, ***b*** and ***c*** for big-wing and ***d***, ***e*** and ***f*** for small-wing. Vortices shed at the end of each strokes are evident in ***a*** and ***c*** for big wing and in ***d***, ***e*** and ***f*** for small wing. In ***f***, a vortex shed in previous stroke (shown in inset) has moved to circled area (right bottom corner) while a new vortex is just shed at the other end. Blue arrows indicate the direction of the fluid flow and black arrows in the top panel indicate the motion of the wing.

In the Figure 2.10, flow fields generated by the wings flapping up and down with symmetrical velocity profiles are shown. Flapping wing generates vortex structures at the end of each stroke, which propel away from the wing. These vortex structures create intermittent jets, alternately, at the each end position of the wing. Due to the symmetry in the flow structure wing experiences reaction-forces in opposite directions resulting in a zero net lift force over a cycle. This observation is very similar to the clap and fling motion of the model wing. Even though in the present case (Figure 2.10), it takes some time for a vortex structure to develop, shed vortices are relatively well defined compared to that in the case of clap and fling arrangement.

Finally, we present flow visualization results for the case of wing flapping with asymmetric velocity profile (Figure 2.4b). In this case, we had down-stroke at higher Reynolds number and upstroke at lower Reynolds number. Even though there is a perceptible

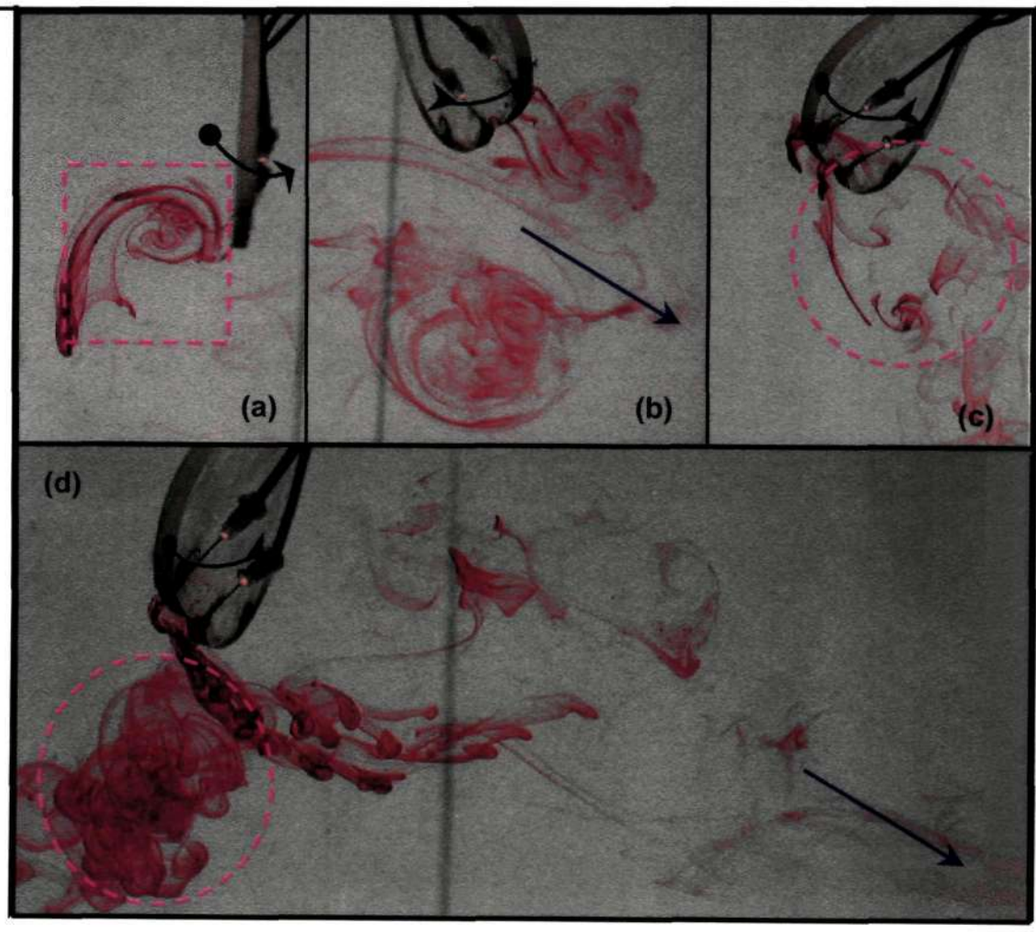

Figure 2.11: Flow visualization pictures for the case of flapping wings with asymmetric velocity profiles. **a** during down-stroke and **b** at the end of down-stroke (Re=1070) and **c** (Re=750) at the end of upstroke. **d** is at the end of upstroke (for this experiment down-stroke Re=1520 and upstroke Re =465). Pink square area indicates well-developed vortex during down-stroke and pink circle indicates the absence of a well-defined vortex. Blue arrows indicate direction of fluid flow, black arrows indicate direction of wing motion.

change in time required to complete up and down strokes in the model, for a butterfly flying with 5 Hz wing beat frequency, the differences in these times are not noticeable (0.0825 s for down stroke and 0.1175 s for upstroke).

Flow visualization pictures have been given in Figure 2.11 and 2.12. In these pictures, one

Figure 2.12: In this figure flow field for a flapping wing with asymmetric velocity profiles (Re-1070-750), after many cycles of operations. Unlike in symmetric flapping, in this case asymmetry in the flow field is clearly evident. Almost all the fluid is displaced in the direction of the blue-arrow starting from upper left corner to the lower right corner. As a result, flow from both wings would produce a net lift force in the direction of the red arrow.

prominent feature that is different from symmetric velocity cases is the appearance of a well developed vortex only in the down-stroke (Figure 2.11 a and b; higher Reynolds number/higher velocity) where as it is absent in the upstroke (Figure 2.11 c and d; lower Reynolds number /lower velocity). In Figure 2.11d, it is evident that the dye is almost stagnant at the left end, where as it is diffused and flushed out at the right end. After many cycles of operation of the test-rig, asymmetric velocity driving of the wings leads an asymmetrical flow field in which fluid is pumped down from upper left corner to the lower right corner as shown in the Figure 2.12. All the above observations indicate that, in the case of asymmetric velocity profile, there is a net force developed during a complete flapping cycle.

Other factor to be highlighted here is that, for a 1-degree freedom system and for the range of Reynolds number considered in this study, we were unable to observe symmetry breaking with symmetric-flapping as indicated by Makoto and Yanagita, (2001). The only way to introduce asymmetry would be to have asymmetric flapping. Even though the asymmetry in flapping is hard to notice, the flow filed shows a dramatic change and there is clear indication of net-lift generation in a flapping cycle. The result is encouraging to explore simple flapping mechanism for the adaptation of MAV.

CHAPTER 3: Experiments With Insects

3.1 Introduction

In this chapter, we present some of the preliminary work done for the study of wing kinematics of a live insect flying in the wind tunnel. The study of insect flight under controlled condition, in a wind tunnel, will help us in understanding relative importance of various unsteady aerodynamic principles for the insect flight under different flying conditions. However, these studies are highly challenging due to following factors:

(a) We need to have high speed video recording to study the wing kinematics of an insect while in flight, typical flapping frequencies are (a) butterfly 5 Hz, (b) dragonfly 30-40 Hz and mosquitoes 300-400 Hz. To study the kinematics of wing motion, one needs to record the flapping-wing motion at least 10 times faster than the wing beat frequency. With the CCD-camera available in our lab, which can go up to a recording speed of 350 Frames/s (FPS), we could study dragonfly and butterfly. To get details of the wing motion in 3-dimensional space, we need develop a recording arrangement to get at least two simultaneous views of the wing motion.

(b) To conduct many experiments on the same insect under different flying conditions, we need to preserve an insect for few days under captivity.

(c) Typical velocities for the insect flight is about 1m/s. Hence we need to operate wind tunnel and measure wind velocity in the low velocity regime using hot wire.

In the following sections we present solutions to above-mentioned problems which would facilitate the insect flight research program.

3.2 Camera arrangement for studying wing-kinematics:

A matchstick is fixed in the thorax region of the insect using super-glue and mounted on to a stand with a double-sided adhesive tape. The stand with the mounted insect is placed inside the wind- tunnel and the position is adjusted so as to locate the insect in the middle of the test-section. Three mirrors and a CCD camera arrangement, as shown in the Figure 3.1, are used to capture the top and back-view of the flying insect. Each of the three mirrors used in the setup has six degrees of freedom, which will facilitate fine adjustment of the positions of the mirrors. The optical path length for a ray entering CCD camera either from the top view or back view is same, this is essential to get sharp images of both views simultaneous using single CCD camera. Illumination of the insect is done using two electric bulbs and the intensity is adjusted (by changing distance and direction of the light source) so as to get uniformly illuminated top and back views. The recorded image in the CCD camera has both

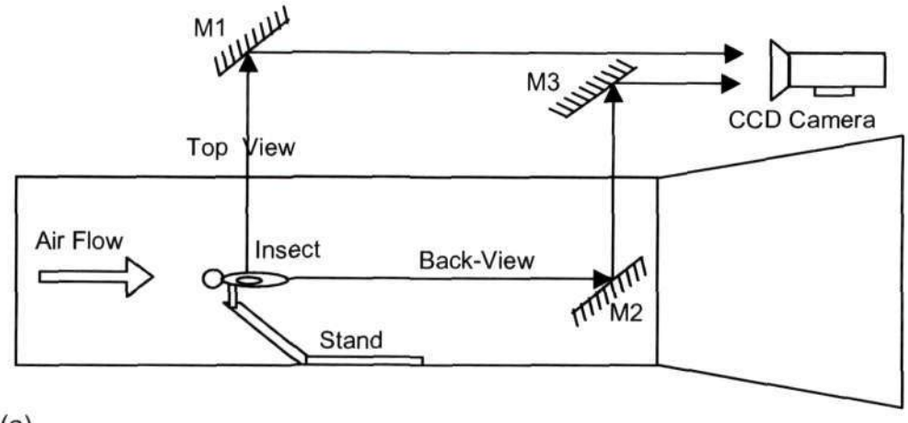

(a)

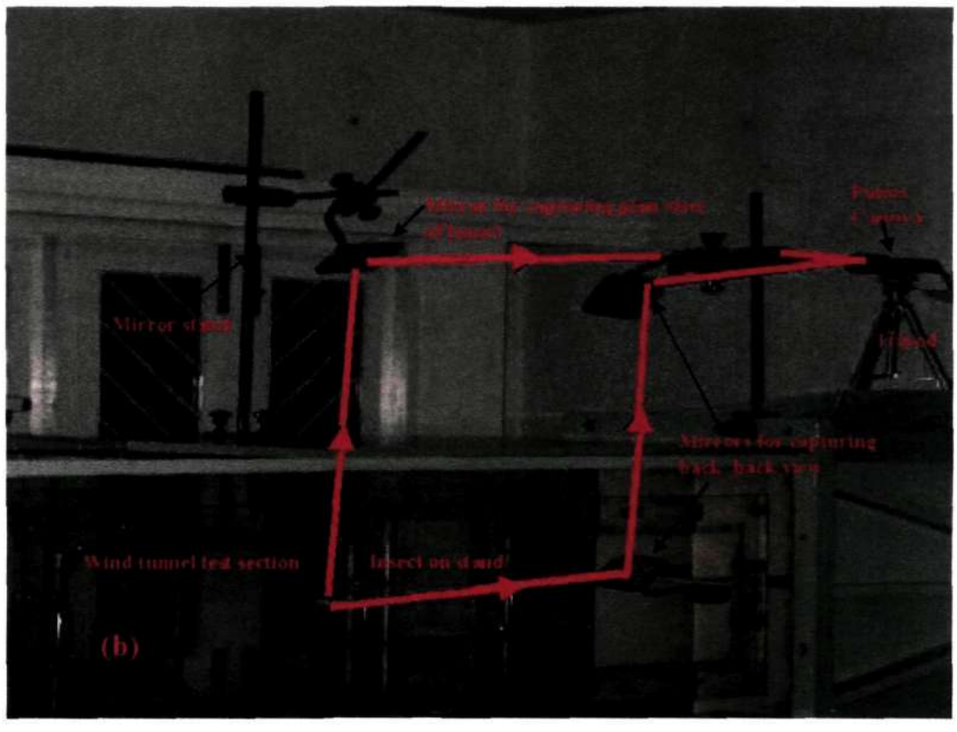

Figure 3.1: (a) Schematic diagram of camera and mirrors arrangement for recording top and back-view, M1, M2 and M3 are mirrors. (b) Photograph of the same arrangement

views in a single frame, top view is recorded in the upper half of the frame and the back-view in the bottom half of the frame.

CCD camera used in the setup is Pulnix® make, TM-6710 model, has a normal resolution of 640 X 480 pixels and it is a monochrome camera. The camera can be used at different frame rates and accordingly the one has to compromise on resolution or the field of view. Some of the possible modes of operation for TM-6710 camera are:

(a) 120 Frames/s 640 X 480 resolution

(b) 240 Frames/s 240 X 480 (2 Rows binned mode, full field low resolution)

(c) 200 Frames/s 200 X 480 (partial scan 200 lines)

(d) 350 Frames/s 100 X 480 (partial scan 100 lines)

Depending on the experimental requirement, we can select any of the above modes of operation of CCD to record wing motion of an insect. Preliminary results obtained for getting simultaneous views of an insect mounted in wind tunnel is shown in Figure 3.2.

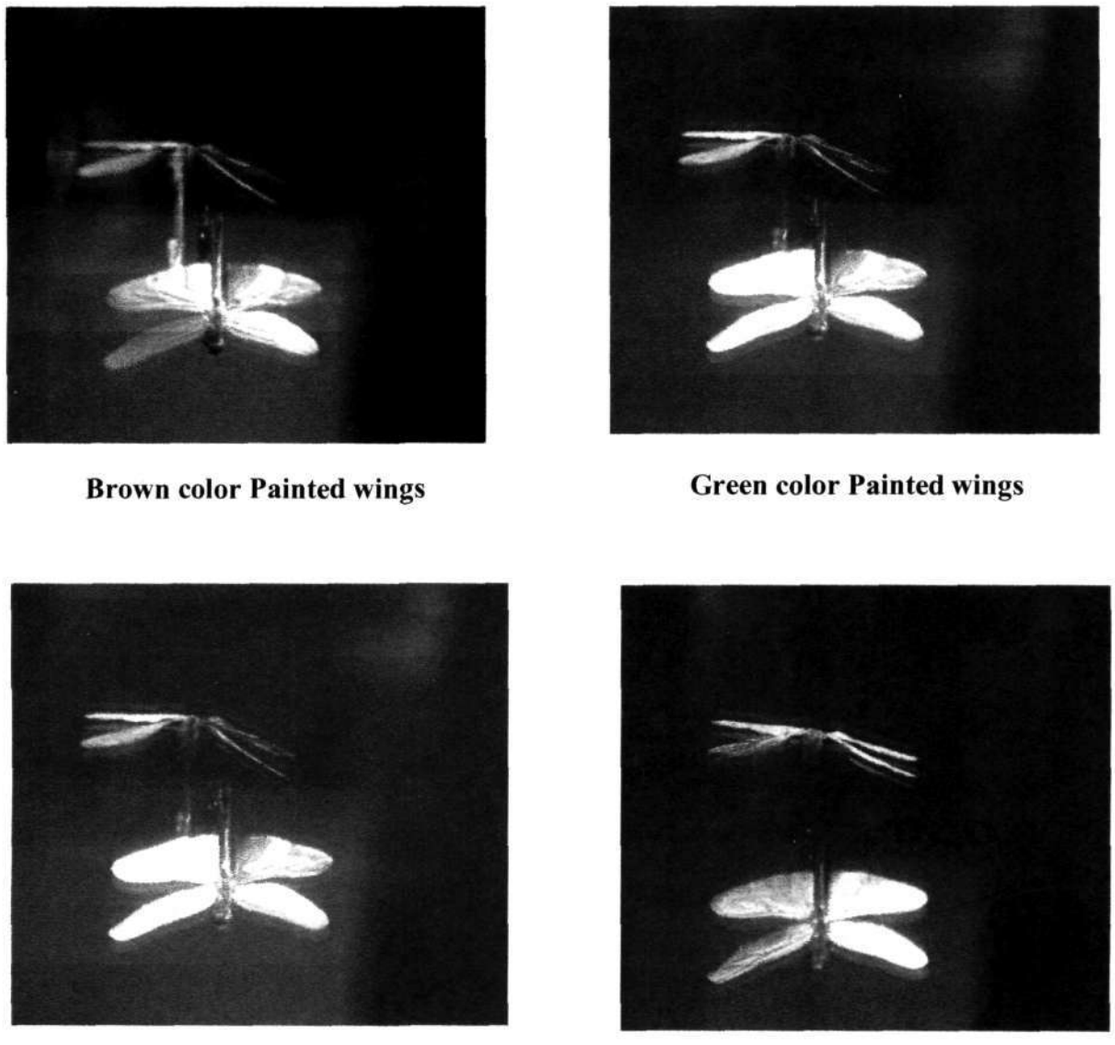

Brown color Painted wings **Green color Painted wings**

White color Painted wings **Silver color Painted wings**

Figure 3.2: Simultaneous recording of top and back views of an insect in the wind tunnel. In this case for developing proper mirror arrangement and lighting arrangements, a dead dragonfly insect used. Frame Rate = 120 frames/sec, Frame Buffer: 20, Exposure Time: 4.0 ms.

We found silver painted wings of a dragonfly gives best contrast. However, we were forced to abandon further experiments because Pulnix camera developed some problems and has to be sent back to USA for repairs.

3.3 Preservation of insects:

Dragonfly is a predator insect and catches its pray while in flight. High maneuverability of dragonfly helps in this aerial hunting. We used insect net to capture the insects for our experiments. Care has to be taken while capturing them so as to avoid damage to their wings. Using light weigh nylon net instead of cloth net is preferable. Many of the dragonflies can be seen over the lawns in our institute, especially after watering of the lawns. We also captured dragonflies from neighboring agriculture university campus (GKVK-campus). Butterflies are mostly captured in our campus. Many experiments need to be carried out under different flight conditions, for the comparison of the data it is desirable to keep captured insects alive for few days and use same insect in a set of experiments.

Dragonflies were provided with mosquito larvae and for the butterflies sugar/honey water solution. When many dragonflies are put in the same box, we observed that they tend to eat weaker once. However we were unable to keep them alive for more than 24 hours in captivity. Even after supplying their food, by the second day, they are unable to fly, and they seem to be completely exhausted. At this point, on the advice of Prof. Alexander (private communication), we kept the insects in a refrigerator. The temperature was maintained around 5 to 9^0 C. Insect with the larvae and cotton-balls soaked in sugar syrup are placed in a box with small breather holes and kept in the refrigerator. Cotton ball will help in maintaining humidity and at lower temperature the rate of metabolism for the insects reduces. With this arrangement we were able to keep dragonflies alive for 2 to 3 1/2 days and butterflies for 4 days (maximum).

Before using these insects in the experiments, they were warmed up gradually to the room temperature and were nourished by providing sugar syrup and/or mosquito larvae. While mounting on the matchstick care has to be taken to ensure that the glue used is not harmful to the insect skin and the glue does not restrict leg, wings and other body parts. Using the above preservation method, we can preserve even insects mounted on the matchstick. After fixing the insect on to the stand we can induce the insect to flap its wing by giving it one smooth touch on its top with a fine painters brush.

3.4 Hot wire anemometer calibration:

The hot-wire anemometer technique which uses a small sensing element having a low response time, high sensitivity and minimal flow interference is one of the most suitable methods adopted for measuring turbulence in fluids.

In the hot-wire anemometer instantaneous magnitude of the convective heat loss from a hot-wire (heated resistance wire) kept in a flow is a measure of the instantaneous local velocity of the flow. This is valid in a flow when only the velocity changes and the other parameters like temperature and density of the fluid are constant. Because of this restriction, hot-wire anemometer is not an absolute probe and requires calibration before its use in an

experiment. The convective heat loss from the wire is reflected as the I^2R loss from the wire (I is the current through the wire and R is the resistance of the wire). Two modes of the operation are possible for hot-wire anemometers. These modes depend on whether current through the wire is kept constant or resistance of the wire is kept constant. In the constant temperature hot-wire anemometer the resistance of the wire is kept constant by an electric feed back arrangement. The conventional constant temperature hot-wire anemometer consists of a Wheatstone bridge, a servo amplifier and a current driver, as shown in figure below. The active arm of the bridge contains the probe. The passive arm contains a variable resistor for

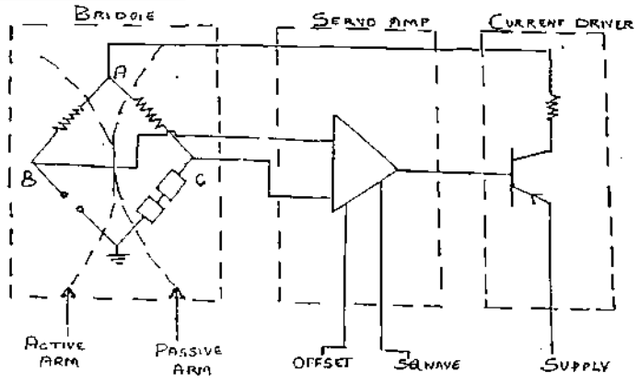

Figure 3.3: Schematics of Constant-Temperature Hot-wire Anemometer

comparison. When the bridge is in balance, no voltage difference exits across BC (bridge output). Any change in the flow across the wire changes the cooling rate of the probe, resulting in the probe becoming cooler or hotter as the case may be. The resultant resistance change due to change in temperature of the wire brings about a voltage difference in the bridge output, which is an. input to the servo amplifier. The output of the servo amplifier drives a current driver which changes the current through the bridge and hence the probe. The phase relation of the current is such that the cooling of the wire increases the current and heating of-the wire decreases it in such a way that change in the resistance of the wire is compensated and the resistance is held very nearly constant. It can easily be seen that higher the servo amplifier gain and a very high slew rate, the lower is the error voltage required across the bridge to compensate for the temperature change (resistance change) of the probe. Higher gain also leads to higher frequency response. Therefore constant temperature anemometer has to be designed carefully to have a large servo amplifier gain and stability.

In the following part of this section we present a procedure to calibrate hot-wire anemometer in the low velocity regime. The velocity range of interest for the insect flight dynamics is from 0 to 2 ms^{-1}. The calibration rig consists of an oscillating cylindrical bar carrying the probe and a data logger. Schematic diagram of the set is given in Figure 3.4.

A circular rod of diameter "d" and length "L" is suspended from a pivot. The anemometer probe is fixed at a distance "l" from the pivot (see Figure 3.4) and is connected to a data logger. When the rod is raised by a distance "h" and released, it will start oscillating. The probe will see a relative air-velocity and the response of the probe is recorded by the data-logger. We can change the maximum velocity of the probe by changing the distance "l" of the probe from the pivot. In the experiment we measure the time period of oscillation of the rod and by which we can compute maximum velocity and the probe response (in voltage) is calibrated. For small angles of displacements (for small h/L) the dynamics of the oscillating rod is like a compound pendulum and is governed by following equation:

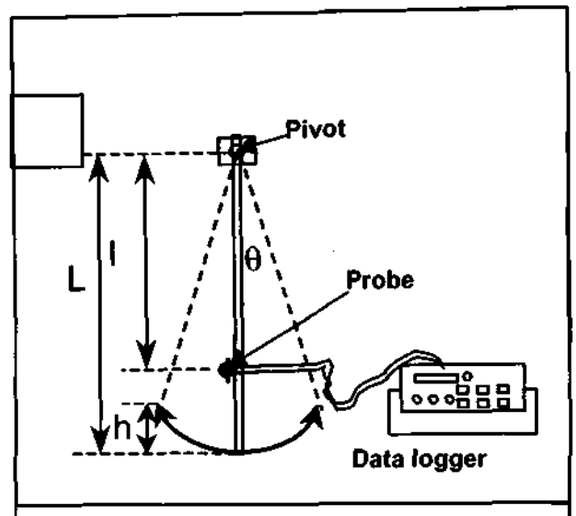

Figure 3.4: Schematic diagram indicating pendulum arrangement for calibrating hot-wire in the low velocity range

$$\frac{d^2\theta}{dt^2} + \frac{I\,g}{2\,I^2}\,\theta = 0 \qquad\qquad I^2 = \frac{d^2}{16} + \frac{L^2}{3} \approx \frac{L^2}{3}$$

Where, θ is the angular displacement "t" is the time and I is the radius of gyration of the pendulum (cylindrical rod) about the pivotal point. Hence, the period of oscillation of the pendulum, τ, is given by following expression.

$$\tau = 2\pi\sqrt{\frac{2\,I^2}{L\,g}} \approx 2\pi\sqrt{\frac{2\,L}{3\,g}}$$

In our setup L=0.98 m and the theoretical value for the period of oscillation is 1.622 sec. In our experiments following observations are done for the period of oscillations:

Number of Oscillations	Time indicated by the stop watch
8	13.15 s
8	13.30 s
8	13.25 s
Avg. time for one Oscillation	1.654 s

The observation is in close agreement with the theoretical value. From the experiments, maximum value of angular velocity, "$\dot{\theta}_m$", can be calculated once we know the angle of displacement θ (through h), time period of oscillations (τ) and using the expression given bellow.

$$\bar{\dot{\theta}} = \frac{4\theta}{\tau} = \frac{4}{\tau}\dot{\theta}_m \int_0^{\tau/4} \cos\left(\frac{2\pi t}{\tau}\right) dt \qquad Or \qquad \boxed{\dot{\theta}_m = \frac{2\pi}{\tau}\,\theta}$$

From the experiments, τ = 1.654s, and θ = 0.3803 (for h =0.07 m), hence the maximum angular velocity will be 1.44 radians/s. We can also obtain the theoretical value of the maximum angular velocity by energy conservation principle. Equate the potential energy of the rod when it is in the extreme position (zero kinetic energy) to the kinetic energy it has at the lowest point (zero potential energy).

$$Mg\frac{h}{2} = \frac{1}{2}MI\ \dot{\theta}_m^2 \qquad Or \quad \dot{\theta}_m = \sqrt{\frac{3gh}{L^2}}$$

Substituting h= 0.07m, g= 9.81 m/s^2 and L=0.98m we get the theoretical value of the maximum angular velocity as 1.464 radians/s. Again theoretical and the experimental values are in close agreement (98.3 % of the theoretical value).

Now after these verifications, we adjust the probe distance "l" from the pivot to get desired value of the velocity using the following expression (same as the above expression, recast in terms of desired velocity "V", raised height of the rod-end, "h", and probe distance "l").

$$l = \frac{VL}{\sqrt{3gh}}$$

In the Figure 3.5, we indicate the probe setting distance from the pivot depending on the desired velocity of the probe (with h =0.3 m).

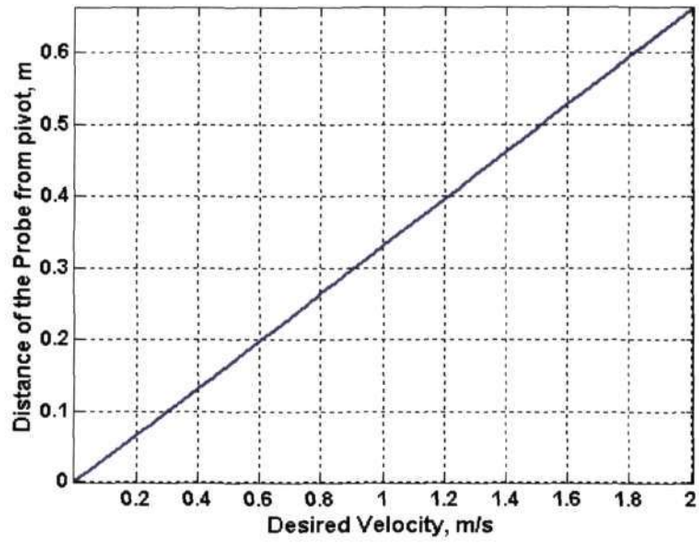

Figure 3.5: Setting of the probe distance depending on the desired velocity. In further experiments we have taken pendulum raise height, "h", equal to 30 cm.

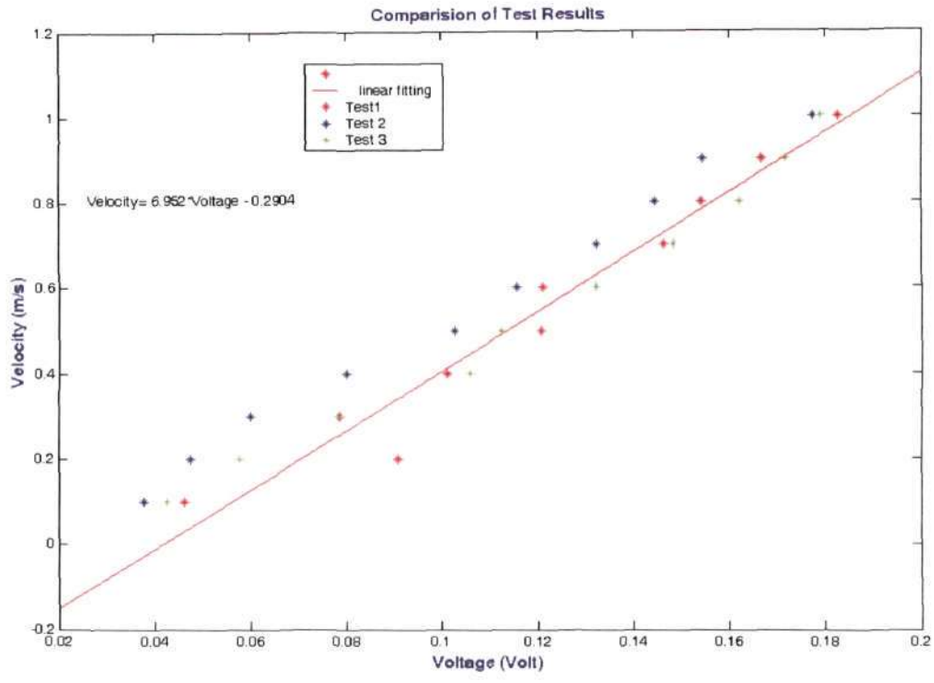

Figure 3.6: Variation of velocity (m/s) of the probe with probe output (voltage). Different tests were done on different days.

Now we present (above) a set of results indicating probe output with the probe velocity which was obtained using the oscillating pendulum arrangement in Figure 3.6.

Hence from our preliminary results we can say that the oscillating pendulum arrangement can be used for calibrating hot-wire anemometer in the low velocity range. Further modification to measure position of the pendulum would greatly enhance the utility of this method.

Chapter 4: Conclusions

In this thesis we have steadied unsteady aerodynamics of insect flight by carrying out flow visualizations experiments using a mechanical test rig to mimic insect flight. We studied (a) clap and fling arrangement, (b) symmetric flapping and (c) asymmetric flapping flight configurations. The only way, we could induce asymmetry in the flow structure and hence a net lift-force generation is by having asymmetric flapping of the wings. With the asymmetric flapping of the wings, even with one degree freedom of the test rig, we were able to generate net lift force. This gives a hope to explore the possibilities of using simple mechanical arrangements (hence lighter weight) for adaptation into the MAV.

We presented some of the preliminary arrangements done for carrying out insect flight studies using live insect flying in a wind tunnel. We were able to develop a preservation procedure to keep dragonfly and butterfly for a period of 3-4 days. We have developed a high speed imaging system to capture simultaneous top and back vies of an insect flying in the wind tunnel. Finally thesis presents a simple oscillating pendulum arrangement for calibration of hot wire anemometer in the low velocity range.

Scope for Further Work:

In understanding unsteady aerodynamics of insect flight we have to relate flow field (by flow visualization and PIV) to the wing kinematics and the instantaneous forces. Hence, the study of live insect to get above set of data and a mechanical device mimicking some the important unsteady aerodynamic effects is useful. Addition of PIV and force data is a challenging exercise, which eventually helps in identifying efficient modes of operating a MAV for a given application.

Appendix

All figures show angular velocity and displacement (Y-axis) variation with time (X-axis) for Asymmetric and Symmetric strokes, with different Reynolds Numbers.

Example: R-2420-1680/1070-750 (Asymmetric)

R = Reynolds Number
R-2420 = Reynolds Number for the Big-wing during downstroke.
R-1680 = Reynolds Number for the Big-wing during upstroke.
R-1070 = Reynolds Number for the Small-wing during downstroke.
R-750 = Reynolds Number for the Small-wing during upstroke.

Time for Asymmetric downstroke(Tad) = 1/2(Time for Asymmetric upstroke (Tau))

Example: R-2420-1070(Symmetric)

R = Reynolds Number.
R-2420 = Reynolds Number for the Big-wing.
R-1070 = Reynolds Number for the Small-wing.

Time for Symmetric downstroke(Tsd) = Time for Symmetric upstroke(Tsu)

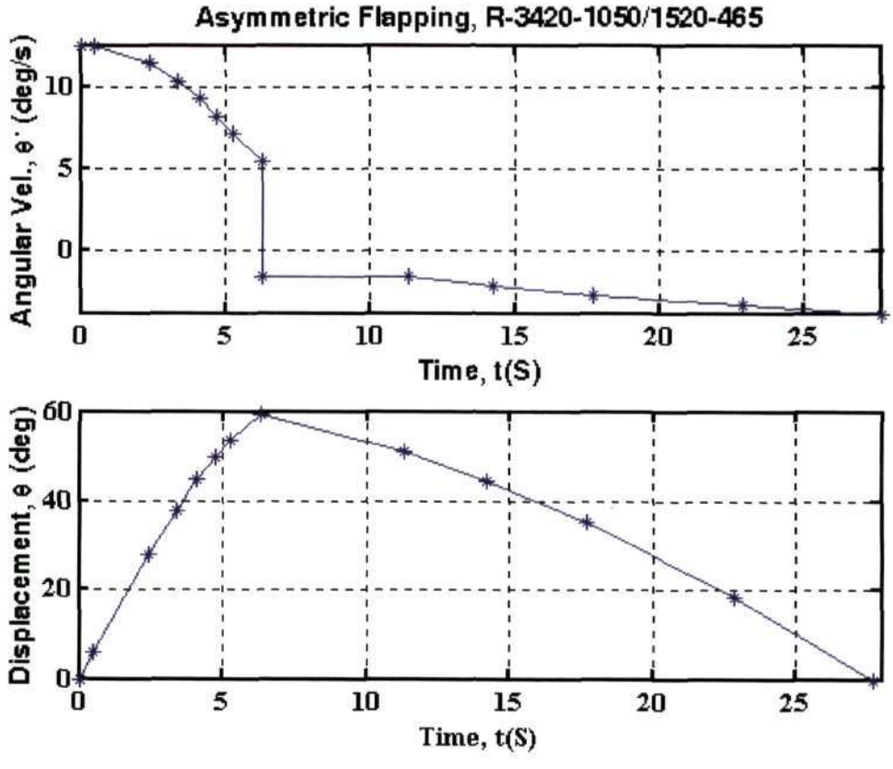

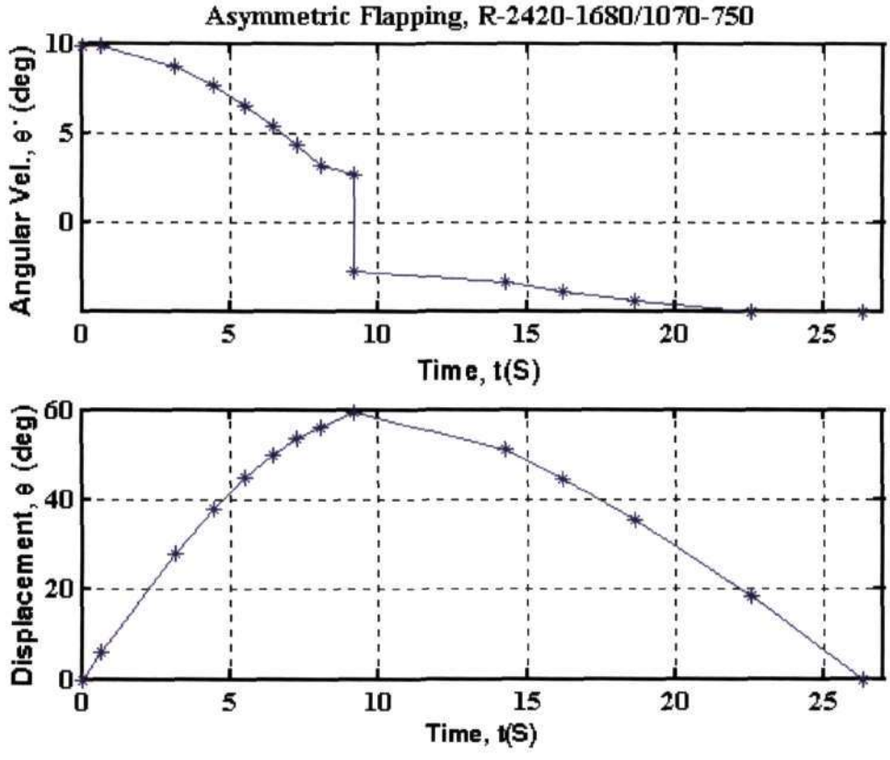
Asymmetric Flapping, R-2420-1680/1070-750
Angular Vel., θ' (deg)
10
5
0
0
5
10
15
20
25
Time, t(S)
Displacement, θ (deg)
60
40
20
0
0
5
10
15
20
25
Time, t(S)

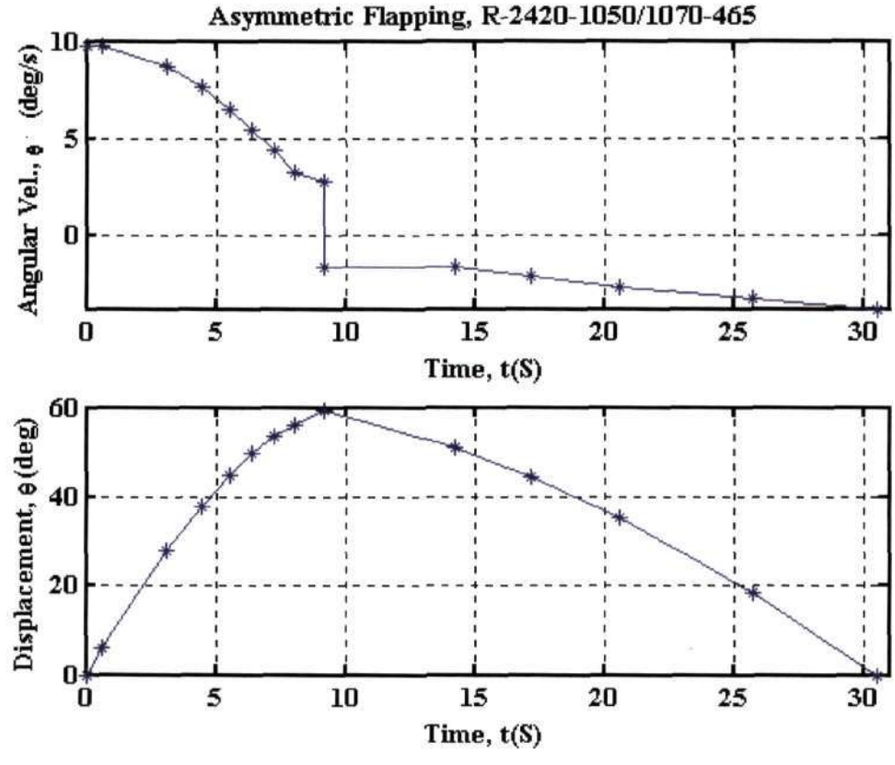
Asymmetric Flapping, R-2420-1050/1070-465
Angular Vel., θ' (deg/s)
10
5
0
0
5
10
15
20
25
30
Time, t(S)
Displacement, θ (deg)
60
40
20
0
0
5
10
15
20
25
30
Time, t(S)

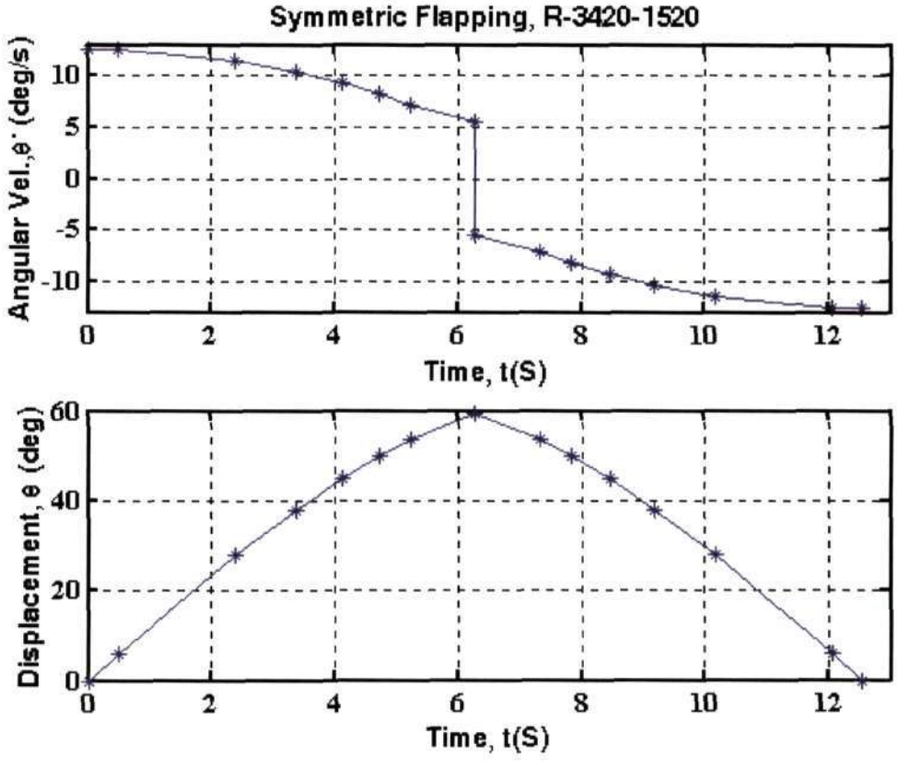
Symmetric Flapping, R-3420-1520
Angular Vel.,θ' (deg/s)
10
5
0
-5
-10
0
2
4
6
8
10
12
Time, t(S)
Displacement, θ (deg)
60
40
20
0
0
2
4
6
8
10
12
Time, t(S)

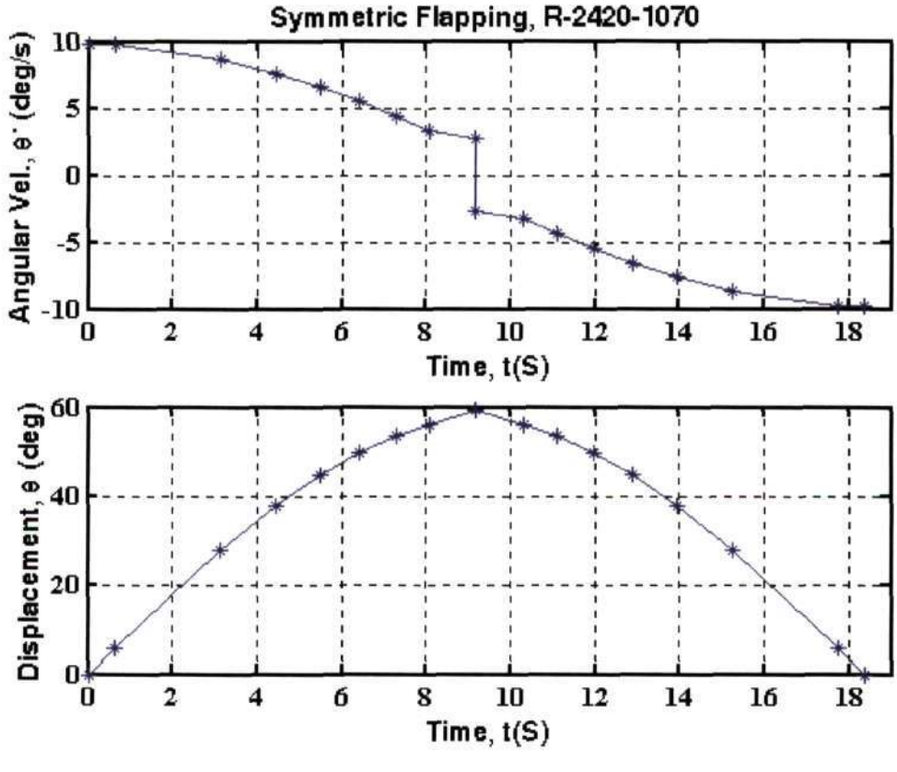
Symmetric Flapping, R-2420-1070
Angular Vel., θ' (deg/s)
10
5
0
-5
-10
0
2
4
6
8
10
12
14
16
18
Time, t(S)
Displacement, θ (deg)
60
40
20
0
0
2
4
6
8
10
12
14
16
18
Time, t(S)

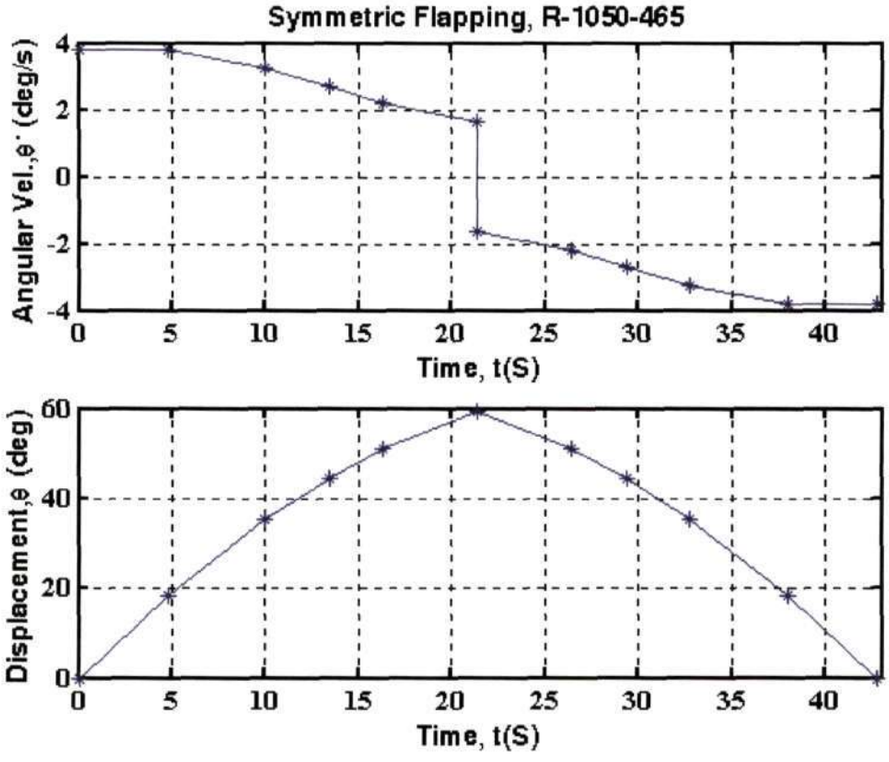

References

C. Maresca, D. Favier and J. Robont, 1979, *"Experiments on an Aerofoil at High Angle of Incidence in Longitudinal Oscillations"*, J. Fluid Mech. V 92, 671-690.

Ellington C. P., 1999, " *The novel Aerodynamics of Insect Flight: Applications to Micro-Air Vehicles"* . J. Exp. Biol. V202, 3439-3448

Ellington C. P., 1984a, *"The Aerodynamics of Hovering Insect Flight. IV. Aerodynamic Mechanisms"*, Phil Trans. R. Soc. Land. B, V 305, 79-113.

Ellington C. P., 1984b, *"The Aerodynamics of Hovering Insect Flight. V. A vortex theory"*, Phil Trans. R. Soc. Land. B, V 305, 115-144.

Ellington C. P., 1984c, *"The Aerodynamics of Hovering Insect Flight. VI. Lift and Power requirements"*, Phil Trans. R. Soc. Land. B, V 305, 145-181

Lehmann, F.-O. and Dickinson, M. H., 1998, *"The control of Wing Kinematics and flight forces in fruit flies"*, J. Exp. Biol., V201, 385-401.

Lighthill, M. J., 1973, " *On the weis-fogh mechanism of lift generation*". J. Fluid Mech., V60 , 1-17.

Lui, H. and Kawachi, K., 1998, *"A numerical study of insect flight"*. J. Comp. Phys. V146, 124.

Makoto Iima and Tatsuo Yanagita, 2001, "Is a Two-dimensional Butterfly Able to Fly by Symmetric Flapping?", JPSJ, V70, No. 1, 5-8

Maxworthy, T., 1979, *"Experiments on the Weis-Fogh Mechanism of Lift Generation by Insects in Hovering Flight Part* 1", *Dynamics of Fling,* J. Fluid Mech. V93, 47-63.

Michael H. Dickinson, Fritz-Olaf Lehmann and Sanjay P. Sane, 1999, *"Wing Roatation and the Aerodynamic Basis of Insect Flight"*, Science, V 284, 1954-1960.

Sotavalta, O. 1947, " The flight-tone (wing stroke frequency) of insects". Acta Entomol. Fenn. V4, 1-117.

Spedding G. R. and M. Maxworthy, 1986," *The generation and circulation and lift in a rigid two-dimensional fling*". J. Fluid Mech. V165, 247-272

Wakeling and Ellington, 1997a, *"Dragonfly flight. I. Gliding flight and steady-state aerodynamic forces"*. J. Exp. Biol, V200,543-556.

Wakeling and Ellington, 1997b, *"Dragonfly flight. II. Velocities, Accelerations and kinematics of flapping flight"*. J. Exp. Biol., V200, 557-582.

Wakeling and Ellington, 1997c, *"Dragonfly flight. III. Lift and Power requirements"*. J. Exp. Biol., V 200, 583-600.

Wei Shyy et al., 1999, Progress in Aerospace sciences, V 35 455-505

Weis-Fogh, T. 1972, " *Energetics of hovering flight in hummingbirds and in Drosophila*". J. Exp. Biol., V 56, 79-104.

Weis-Fogh, T., 1973, *"Quick Estimates of Flight Fitness in Hovering Animals, Including Novel Mechanisms for Lift Production"*, J. Exp. Biol., V 59, 169-230.

Wilkerson, R.C. and J.F. Butler. 1984, *"The Immelmann Turn, a pursuit maneuver used by hovering male Hybomitra hinei wrighti"*. Ann. Entomol. Soc. Am. V77: 293-295

Wilkin, P. J. and Williams, M. H., 1993, *"Comparision of the aerodynamic forces on a flying sphingid moth with those predicted by quasi-steady theory"*. Physiol. Zool. V66, 1015-1044.

Wortmann, M. and Zarnack, W., 1993, *"Wing movements and lift regulation in the flight of desert locusts"*. J exp Biol, V182, 57-69.

Z. Jane. Wang, 2000, *"Vortex shedding and frequency selection in flapping flight"*. J. Fluid. Mech.V410, 323-341.

Zanker, J. M., 1990, " *The wingbeat of Drosophila melanogaster. I. Kinematics*". Phil. Trans. R. Soc. Lond. B, V 327, 1-18.